REGULAR ARTICLE

The O + O₂ reaction: quantum detailed probabilities and thermal rate coefficients

**Sergio Rampino · Dimitris Skouteris ·
Antonio Laganà**

Abstract The detailed quantum probabilities of the
$O + O_2$ reactive system have been computed at zero total
angular momentum using the time-independent quantum
program ABC thanks to the restructuring of the code and
its implementation on the EGEE production Grid. Their
main features are discussed and out of them *J*-shifting
thermal rate coefficients have been computed to compare
with the experiment and quasiclassical trajectory results
over a wide range of temperatures.

Keywords Oxygen gas phase exchange reaction ·
Relaxed potential surfaces ·
Atom diatom reactive scattering · Quantum rate coefficient

1 Introduction

The calculation of reactive properties of the $O + O_2$ system
is important on the theoretical side to understand the role
played by insertion and abstraction processes in enhancing
and/or suppressing reactivity and on the experimental side

Dedicated to the memory of Professor Oriano Salvetti and published
as part of the Salvetti Memorial Issue.

S. Rampino (✉) · A. Laganà
Dipartimento di Chimica, Università di Perugia,
Via Elce di Sotto 8, 06123 Perugia, Italy
e-mail: ser_ram@dyn.unipg.it

A. Laganà
e-mail: lag@dyn.unipg.it

D. Skouteris
Dipartimento di Matematica e Informatica,
Università di Perugia, Via Vanvitelli 1,
06123 Perugia, Italy
e-mail: dimitris@dyn.unipg.it

to control the reaction chains involved in combustion.
As to the theoretical aspects, a large amount of literature
has been recently devoted to the analysis of the distinctive
features of different reactive mechanisms [1–3]. As to
combustion applications, quasiclassical trajectories have
been run to evaluate vibrational deexcitation and thermal
rate coefficients for the exchange reaction and dissociation
rates [4–8].

However, due to the complexity of the electronic
structure of the oxygen atom oxygen molecule system and
to its heaviness, very little work has been reported in the
literature on the calculation of the thermal rate coefficient,
that is, instead, the experimental data to compare with [9].
For this purpose, we ran (as we did also in the past for a
comparison with approximate quantum methods [6]), the
quasiclassical trajectory (QCT) ABCTraj program [10].
For the same reason, we ran also the quantum time inde-
pendent ABC program [11]. This allowed us to calculate
the zero total angular momentum reactive probabilities and
work out the value of the thermal rate coefficient using a
J-shifting model. The calculations were performed on the
production computing Grid segment of EGEE [12] made
available to the Virtual Organization (VO) COMPCHEM
[13], using the potential energy surface of [5].

Accordingly, the paper is organized as follows: in
Sect. 2 the potential energy surface is described, with
particular attention to its relaxed representation on proper
sets of coordinates. In Sect. 3, the quasiclassical and
quantum treatments are outlined with specific reference to
their implementation on the production European Grid
infrastructure. In Sect. 4, computed quantum detailed
probabilities are discussed and the thermally averaged rate
coefficients evaluated out of them are compared with val-
ues obtained from the experiment and QCT calculations.
Conclusions are drawn in Sect. 5.

2 The potential energy surface

2.1 The DMBE potential

The single valued potential energy V used for the calculations is formulated as a semiempirical double many body expansion (DMBE) [14, 15] having the general form

$$V = \sum_{i}^{3} V_{EHF,i}^{(2)} + V_{EHF}^{(3)} + \sum_{i}^{3} V_{corr,i}^{(2)} + V_{corr}^{(3)}. \quad (1)$$

In the DMBE formulation, both the two-($V^{(2)}$) and the three-($V^{(3)}$) body components of the interaction are partitioned into an extended Hartree–Fock ($V_{EHF}^{(n)}$, including the non-dynamical correlation of the valence electrons in open shells or nearly degenerate orbitals) and a dynamical correlation ($V_{corr}^{(n)}$) term (arising from the dynamical correlation of the electrons). Ab initio SCF potential energy values (or a function parametrized to available spectroscopic data) are used to represent $V_{EHF}^{(n)}$ while $V_{corr}^{(n)}$ is obtained semiempirically, by an interpolation from dispersion energy coefficients of the various asymptotic channels of the potential surface. A complete description of the DMBE functional form used for the O_3 PES is given in [5].

The key features of an atom diatom reactive PES can be illustrated using the so called "relaxed" isoenergetic contour plots [16]. In the relaxed plots of V for three atom (A, B and C) systems two coordinates are taken as the independent variables of the graph and the third one is varied (relaxed) to reach a minimum of the potential. In [5] for the A = B = C = O system use was made of the reduced symmetry (RS) coordinates Q_2^* and Q_3^* defined as

$$Q_2^* = \frac{s_2/s_3}{\sqrt{2}} \quad Q_3^* = \frac{2s_1 - s_2 - s_3}{\sqrt{6}} \quad (2)$$

where $s_i = r_i / \sum_{j=1}^{3} r_j$ (with $r_1 = r_{AB}$, $r_2 = r_{BC}$, $r_3 = r_{AC}$) and the relaxed variable is the perimeter p of the molecular triangle [17].

2.2 The perimeter relaxed plots

The resulting perimeter relaxed plot (hereinafter called p-relaxed RS plot) of the isoenergetic contours of the O + O_2 DMBE PES shown in Fig. 1a is constructed by varying the perimeter from 1 to 30 bohr. The associated values of the relaxed perimeter are plotted in Fig. 1b. As shown by Fig. 1b, the relaxed geometry is associated with large perimeters at the three corners of the triangle (implying that the more asymptotic arrangements are preferred as confirmed by the associated V values plotted in Fig. 1a). By moving inwards or along the sides, arrangements with smaller perimeter values are preferred (implying that the more tightly bound arrangements are
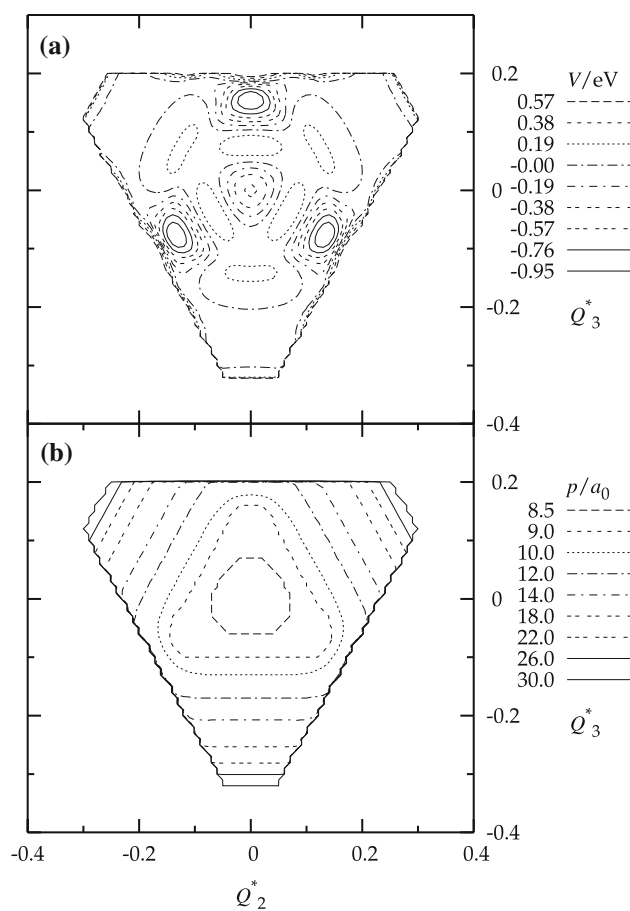

Fig. 1 a p-relaxed RS plot of the isoenergetic contours of the O_3 DMBE PES. Energy contour values are given in eV. Zero energy is taken as the O + O_2 asymptote. **b** contours of the values of the relaxed perimeter (bohr)

preferred). From an inspection of Fig. 1a one can figure out possible minimum energy paths (MEPs) connecting reactants to products in going from collinear (sides of the triangle) to perpendicular (center of the triangle) atom-diatom approaches. Particularly well illustrated are the MEPs connecting the three equivalent minima associated with the C_{2v} equilibrium O_3 structures (separated from each other by a rotation of 120°) and the ones connecting them to the minimum at $Q_2^* = Q_3^* = 0$ associated with an equilateral D_{3h} O_3 geometry. The exchange reaction path going through a C_{2v} minimum, though not well resolved in the plot, shows to require no activation energy while the C_{2v} to D_{3h} isomerization requires dissociation. The associated perimeter contours tell us that the triangle formed by the three oxygen atoms becomes increasingly more compact when approaching geometries typical of half the reaction and that its size becomes minimum at geometries away from collinearity.

2.3 The HYBO relaxed plots

As seen above, a close inspection of the p-relaxed RS plots singles out their little suitability to describe reactive events. This is due to the fact that they do not render in a simple intuitive way most of the features of the various paths leading from the reactant to the product asymptote. On the contrary, a reaction oriented picture of the PES is the one making use of the hyperspherical bond order (HYBO) coordinates [18, 19]. The bond order (BO) variables are defined as $n_i = \exp[\beta(r_{i\text{eq}} - r_i)]$ with $i = $ AB, BC, CA. For the $A + BC$ $(v, j) \rightarrow AB$ $(v', j') + C$ process (vj is the reactant vibrational state, $v'j'$ is the product vibrational state), the HYBO coordinates obtainable out of the BO variables are defined as

$$\rho = \sqrt{n_{\text{BC}}^2 + n_{\text{AB}}^2} \quad \alpha = \arctan \frac{n_{\text{BC}}}{n_{\text{AB}}} \tag{3}$$

and the approaching angle Φ is $\hat{ABC}$. The HYBO coordinates are better suited for a description of the reactive process. ρ has in fact a clear stretching nature (one has to bear in mind here that the BO space is inverted with respect to the physical one because $n = 0$ corresponds to an infinite internuclear distance and $n = \exp[\beta r_{\text{eq}}]$ corresponds to a zero internuclear distance) and α has the clear nature of a reaction coordinate smoothly connecting the reactant arrangement ($\alpha = 90°$) to the product one ($\alpha = 0°$).

These features make the HYBO coordinates appealing for use in dynamics calculations. In fact, despite the higher complexity of the Hamiltonians written using non-orthogonal coordinates [20], bond length coordinates have been succesfully used for scattering calculations for the prototype collinear system $H + H_2$ [21].

A relaxed representation based on HYBO coordinates is discussed in detail in the forth-coming paper "Microscopic branching processes: the $O + O_2$ reaction and its relaxed variable representations" submitted for publication to the *International Journal of Quantum Chemistry*. This representation makes use of Φ and η (with $\eta = \pi/4 - \alpha$) as independent variables while relaxing $v = 1 - \rho$ (v can be considered as a generalized reduced symmetry variable gradually evolving from the reactant to the product vibrational coordinate). This type of representation (hereinafter called v-relaxed HYBO plot) is clearly tailored to suit a single process (the $A + BC \rightarrow AB + C$ one in our case) for which Φ varies from $180°$ (collinear attack of A to B on the side of B) to $360°$ or $0°$ (collinear attack of A to B on the side of C).

2.4 The analysis of the $O + O_2$ reactive paths

The v-relaxed HYBO plots for the $O + O_2$ system obtained using the values of the BO variables ($\beta = 1.7407a_0^{-1}, r_{\text{eq}} = $

2.2818a_0) of [18], are shown in Fig. 2 (upper panel for isoenergetic contours, lower panel for relaxed v values contours). In the plot, one can easily see that the most favoured angle for reactive attacks is about $135°$, in which, however, at half the way to products O_3 tends to form a stable isosceles ($\Phi \simeq 120°$) triangle (see also the lower panel of Fig. 2 by bearing in mind that $v = 0$ corresponds to diatomic distances (at least one) near equilibrium and that as v goes to 1 the internuclear distances tend to infinity). Along this path as the O atom approaches the target molecule, O_2 stretches (the relaxed value of v does not become enough negative) without giving rise to a potential energy barrier. As apparent from the figure, apart from a mild distortion of the triangular shape (a slight decrease of Φ), this path represents the most straightforward way of getting reaction. The figure shows also a second reactive path that leads to a slightly more energetic intermediate. This intermediate is equilateral and about 0.5 eV less stable than the isosceles one. A feature of this
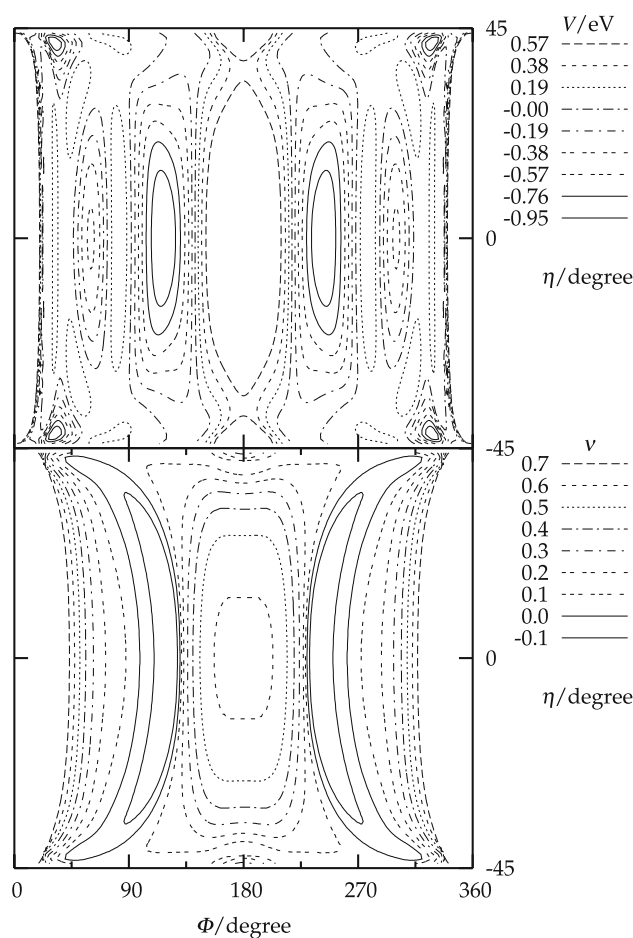

Fig. 2 *Upper panel* v-relaxed HYBO plot of the isoenergetic contours of the O_3 DMBE PES. Energy contour values are given in eV. Zero energy is taken as the $O + O_2$ asymptote. *Lower panel* contours of the values of the relaxed v

path is the double barrier structure sandwiching the well. The collinear MEP is instead highly repulsive at both $\Phi = 180°$ and $\Phi = 0°$ or $360°$. The v-relaxed HYBO plot singles out also two wells at both the top and the bottom corners. These wells are associated with the forming of a stable isosceles complex when A attacks an atom of BC diatom from the opposite extreme ($\Phi \simeq 30°$). The contour plot of the relaxed v values shows also that the attacking A atom can easily move around (relaxed v values gradually become lower than 0) to allow isomerization to the $\Phi \simeq 120° C_{2v}$ complex.

3 The computational machinery

3.1 The Grid parameter study

There are different ways of carrying out the dynamical evaluation of a thermal rate coefficient. In the following, we shall consider only the classical and the quantum methods by focusing on their features relevant to the code gridification.

As already mentioned, in fact, the present study was made possible by an intensive exploitation of the Grid, that is the modern paradigm of high throughput computing. A general scheme for the concurrent reorganization of the related computer programs on the Grid is the following: a distribution procedure iterates over different "events" (which are in our case made of a recursive integration of some differential equations starting from a set of given initial conditions like initial quantum states or energies). Accordingly, the computation is articulated as a coarse grained uncoupled loop that is usually called "parameter sweep". To this end, a procedure able to handle large sets of jobs was developed. Each job execution requires the sending to the Grid of an execution script, of a specific input file and of the scattering programs. The execution script is the same for all jobs while the input file is different for each job. In order to better cope with the heterogeneous nature of both the computing hardware and software (compilers, libraries, submission systems, etc.) of the Grid, executable programs rather than source ones were distributed over the net. In fact, despite the fact that the time required for sending the source code is considerably shorter than that required for sending its executable version (this procedure is more selective in terms of the type of machine to adopt) this approach exploits the fact that there is no need for identifying the compiler of each machine, selecting the optimal options for compilation, compiling the code and verifying that all runs give exactly the same results as the ones obtained on the original machine.

3.2 The quasiclassical dynamics distributed tasks

In QCT studies the distributed computational tasks are those integrating blocks of fixed translational energy (E_{tr}) trajectories starting from a fixed vj value characterizing the vibrotational state of the reactants (all the other initial conditions are selected pseudo randomly). The state (vj) to state ($v'j'$) reactive probability $P_{vj,v'j'}(E_{tr})$ is then calculated as the fraction $N_{vj,v'j'}(E_{tr})/N_{vj}(E_{tr})$ of trajectories ending with a final product vibrational energy associable (even if approximately) to the $v'j'$ state of the products out of the ensemble $N_{vj}(E_{tr})$ of all the trajectories starting from the chosen vj initial state. In our study, use was made of the already mentioned ABCTraj library program [10].

3.3 The quantum dynamics distributed tasks

In the quantum study, as already mentioned, use was made of the program ABC [11]. ABC is based on a time independent hyperspherical coordinate method that integrates the atom-diatom Schrödinger equation for a reaction occurring on a single PES within a Born–Oppenheimer scheme for all the reactant states of a given total energy E. In the quantum distibuted computational tasks, the total energy is the parametric variable employed for gridification.

In the approach adopted by ABC (based on the formalism illustrated in [22]), at each E value the nuclei wavefunction ψ is expanded in terms of the hyperspherical arrangement channel (τ) basis functions $B^{JM}_{\tau v_\tau j_\tau K_\tau}$. The number of basis functions has to be sufficiently large to include all the channels open at the maximum internal energy (emax). These functions are labeled after J (the total angular momentum quantum number, called jtot), M and K_τ (the space- and body-fixed projections of the total angular momentum **J**), v_τ and j_τ (the τ asymptotic vibrational and rotational quantum numbers, with jmax being the maximum value of j considered in any channel), and depend on both the three Euler angles and the internal Delves hyperspherical angles. In order to carry out the fixed E propagation of the solution from small to asymptotic values of hyperradius ρ (not to be confused with the ρ of the HYBO coordinates since ρ is now defined as $\rho = (R^2_\tau + r^2_\tau)^{1/2}$, with $\mathbf{R}_\tau$ and $\mathbf{R}_\tau$ being the Jacobi vectors forming the angle Θ_τ and R_τ and r_τ being the related moduli) we need to integrate the equations

$$\frac{d^2\mathbf{g}(\rho)}{d\rho^2} = \mathbf{O}^{-1}\mathbf{U}\mathbf{g}(\rho). \tag{4}$$

In Eq. 4 $\mathbf{g}(\rho)$ is the matrix of the coefficients of the expansion of ψ, $\mathbf{O}$ is the overlap matrix defined as

Table 1 Input parameters of ABC

jtot	0	Total angular momentum
jpar	−1	Diatomic parity
emax	2.5 eV	Maximum internal energy in any channel
jmax	125	Maximum rot. quantum number in any channel
rmax	12.0 a_0	Maximum hyperradius
mtr	150	Number of propagation sectors
dnrg	0.0005 eV	Energy step

$$O_{\tau v_\tau j_\tau K_\tau}^{\tau' v'_\tau j'_\tau K'_\tau} = \left\langle B_{\tau v_\tau j_\tau K_\tau}^{JM} \middle| B_{\tau' v'_\tau j'_\tau K'_\tau}^{JM} \right\rangle, \tag{5}$$

and **U** is the coupling matrix defined as

$$U_{\tau v_\tau j_\tau K_\tau}^{\tau' v'_\tau j'_\tau K'_\tau} = \left\langle B_{\tau v_\tau j_\tau K_\tau}^{JM} \middle| \frac{2\mu}{\hbar^2}(\bar{H} - E) - \frac{1}{4\rho^2} \middle| B_{\tau' v'_\tau j'_\tau K'_\tau}^{JM} \right\rangle, \tag{6}$$

with μ being the reduced mass of the system and $\bar{H}$ the set of terms of the Hamiltonian operator not containing derivatives with respect to ρ. In ABC, the integration of Eq. 4 is performed by segmenting the ρ interval into mtr ρ sectors inside each and through which the solution matrix is propagated from the ρ origin to its asymptotic value where the **S** matrix is determined [23]. The quantum **P** scattering probability matrix (whose elements are the square moduli of the state to state **S** matrix elements according to the relationship $P_{vj,v'j'}(E) = |S_{vj,v'j'}(E)|^2$) are then calculated for an arbitrarily fine grid of total energy values (Table 1).

3.4 The spin symmetrised probabilities

Strictly speaking, if A, B and C are indistinguishable atoms, the above mentioned scattering probability matrix **P** does not satisfy the Pauli principle since the wavefunction is not appropriately symmetrised. For the case A = B = C = ^{16}O ($I = 0$) the nuclear spin symmetry is A_1 in the S_3 permutation group (A_1 has to be the overall symmetry as well because nuclei are bosons). Therefore, all the six permutations of the original wavefunction have to be added and normalised in order to obtain the A_1 symmetry of related properties including the state to state dynamical information. In doing so, one has

$$P_i = P_{el} + 4P_{ex} + 4\text{Re}(S_{el}^* S_{ex}), \tag{7}$$

rather than

$$P_d = P_{el} + 2P_{ex}, \tag{8}$$

where the subindices i and d mean, respectively, indistinguishable and distinguishable atoms and the subindices el and ex mean elastic and exchange. This means that the exchange contribution is double weighed (i.e. there is a probability transfer from even product rotational states to odd ones, because the former are not considered in an

indistinguishable atoms calculation) and an extra term taking care of the interference between elastic and exchange processes needs to be included.

4 Probabilities and rate coefficients

4.1 The effect of spin symmetrization

Fully symmetrised probabilities calculated for the rovibrational ground $v = 0$, $j = 1$ reactant state to the $v' = 0$, $j' = 1$ product state using Eq. 7 are given in the upper panel of Fig. 3 plotted as a solid line where they are also compared with the values obtained for distinguishable atoms (Eq. 8) and plotted as a dashed line. Figure 3 confirms that there is a strong interference effect. However, when considering the $v = 0, j = 1 \rightarrow v = 0$ state-to-rotationally averaged state (summed over all j') probabilities (see the central panel of Fig. 3) the interference effect is hardly appreciable. A more quantitative comparison of the importance of this effect in the i and d cases is given in the lower panel of Fig. 3, where the plot of the ratio $|P_i - P_d|/(P_i + P_d)$ is given. The figure shows that while for the state to state case (solid line) the ratio is large at all values of energy this is not true for the product rotation averaged case (dashed line), where it rarely exceeds 0.1. For this reason, when performing extended calculations, the spin statistics correction was not considered.

4.2 The effect of collision energy

To put on a more quantitative foot the qualitative arguments brought forward in Sect. 2 when inspecting relaxed representations of the potential energy surface, we investigated the effect on the reaction probability of both vibrationally and rotationally exciting the reactant molecule. State specific probabilities (excitation functions) for $v = 0$, $j = 1$ (solid line), $v = 1$, $j = 1$ (dashed line), and $v = 0, j = 29$ (dashed dotted line) are plotted in Fig. 4 as a function of the translational energy (rather than total energy in order to better single out threshold effects). As apparent from the figure, at $v = 0, j = 1$ the excitation function rises sharply already at zero translational energy as typical of processes with no barrier to reaction. Figure 4 shows also that this high reactivity effect dies off fairly rapidly when collision energy increases (along a no-barrier MEP the process becomes too fast already at fairly low collision energy to allow a significant energy transfer from reactants to products). At higher translational energies, instead, another more slowly rising with energy contribution to the excitation function typical of reaction paths having a barrier comes into play.
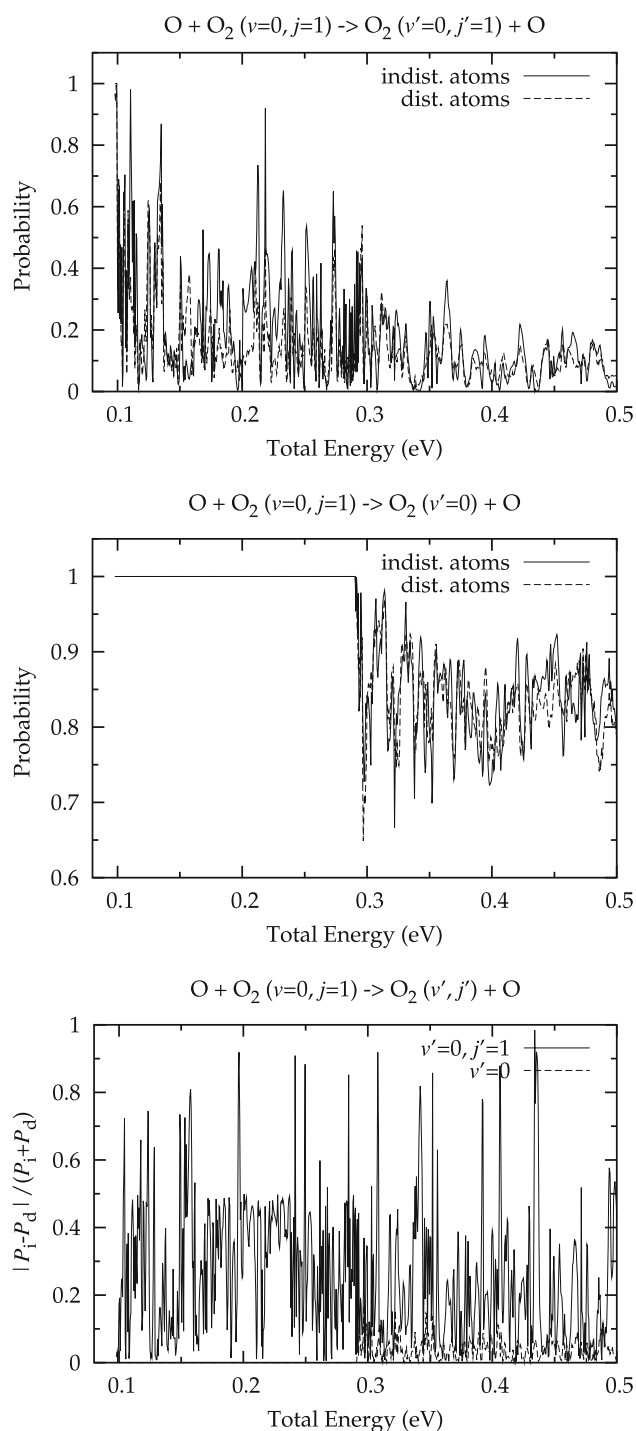
O + O$_2$ ($v=0, j=1$) -> O$_2$ ($v'=0, j'=1$) + O

O + O$_2$ ($v=0, j=1$) -> O$_2$ ($v'=0$) + O

O + O$_2$ ($v=0, j=1$) -> O$_2$ (v', j') + O

Fig. 3 $J = 0$ state ($v = 0, j = 1$) to state ($v' = 0$, $j' = 1$, *upper panel*) and to rotationally averaged state ($v' = 0$, all j, *central panel*) reaction probability plotted as a function of total energy (energy spacing 0.0005 eV) calculated using basis functions with asymptotic maximum internal energy 2.5 eV. In the *lower panel* the interference effect—formulated as $|P_i - P_d|/(P_i + P_d)$ with i and d labeling the indistinguishable and distinguishable particles case, respectively—is shown
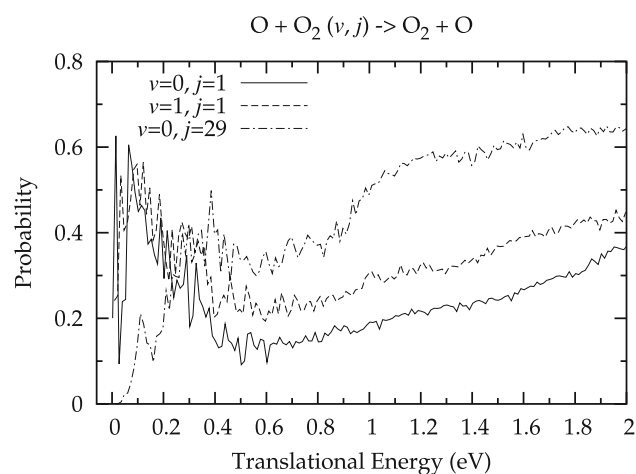

O + O$_2$ (v, j) -> O$_2$ + O

Fig. 4 State specific reaction probability plotted as a function of translational energy (energy spacing 0.0125 eV) calculated using basis functions with an asymptotic maximum internal energy of 3.5 eV. *Solid line* $v = 0$, $j = 1$ ($E_{vj} = 0.09786$ eV); *dashed line* $v = 1$, $j = 1$ ($E_{vj} = 0.29026$ eV); *dashed dotted line* $v = 0$, $j = 29$ ($E_{vj} = 0.25219$ eV)

4.3 The effect of internal energy

When increasing the vibrational excitation of the reactant molecule from $v = 0$ to $v = 1$ (while keeping the rotational state unchanged) the sharp rise to a maximum at zero translational energy followed by a substantial decrease to a minimum of the excitation function remains substantially unaltered. On the contrary, the slowly increasing tail becomes about 0.1 larger. At the same time, a rotational excitation of the reactant O$_2$ to $j = 29$ (that is comparable in energy with the vibrational excitation to $v = 1$) alters significantly the shape of the excitation function. In the state ($v = 0$, $j = 29$) specific probability plot, in fact, the sharp increase at zero translational energy disappears (a kind of residual footprint of this structure survives as a broad bump around 0.4 eV) while the overall shape becomes more typical of reactive processes occurring through the overtaking of a barrier. This supports the already made association of the missing threshold effect for the low j value excitation functions with a barrierless MEP and the interpretation of the high energy increase of the probability in terms of the opening of a different reaction channel going through the surmounting of a barrier as indicated by the inspection of the relaxed HYBO plots in Sect. 2.

4.4 The thermal rate coefficients

The thermal rate coefficient can be calculated from the cumulative reaction probabilities [CRPs or $N(E)$]. $N(E)$ is

obtained from a summation of the detailed state to state reaction probabilities $N(E) = \sum_v \sum_j \sum_{v'} \sum_{j'} P_{vj,v'j'}(E)$ that applies to both quantum and quasiclassical (once a conversion from E_{tr} to E is made) probabilities. Then the thermal rate coefficient can be evaluated using the expression

$$k(T) = \frac{1}{hQ_R} \int\limits_0^\infty e^{-E/k_B T} N(E) dE, \qquad (9)$$

where h is the Planck's constant, k_B is the Boltzmann constant, and Q_R is the reactant (atom diatom) partition function (translational, rotational, and vibrational) at temperature T per unit volume. However, while converged QCT calculations are nowadays easily doable, the exact quantum evaluation of the CRPs is still computationally very expensive and difficult to carry out even on the computing Grid, due to the increasingly larger number of states to be included in the expansion of the wavefunction as J increases. To overcome this limitation, usually the quantum $N(E)$ is expressed in terms of the $J = 0$ one ($N^{J=0}(E)$) using a J-shifting approximation [24]

$$N(E) = \sum_{J=0}^\infty (2J + 1) N^{J=0}(E - \Delta E^{JK}), \qquad (10)$$

where

$$\Delta E^{JK} = \bar{B} J(J + 1) + (A - \bar{B})K^2 \qquad (11)$$

and $\bar{B} = (B + C)/2$, with A, B and C being the rotational constants of the transition state (for the sake of simplicity the geometry of the system at the transition state is assumed to be a symmetric top one).

Since the MEP of the O + O₂ DMBE PES has no barrier to reaction, the point associated with the top of the J-dependent centrifugal barrier was taken as the transition state of the reactive process [25]. To the end of determining this point, we first calculated the minimum energy path along the atom diatom Jacobi coordinate R_τ. Then we added the centrifugal term $\hbar^2 J(J + 1)/(2\mu R_\tau^2)$ and located the first maximum of the curve when moving inwards from the asymptote. At this point for each value of J a triple of A, B and C rotational constants was then calculated for use in Eq. 11.

4.5 A comparison with the experiment

Calculated quantum values of the thermal O + O₂ rate coefficient are plotted in Fig. 5 as a function of temperature in the interval ranging from $T = 300$ to $T = 2000$ K. The results show a nice single exponential behaviour in the range of temperature considered which corresponds to a linear dependence of $\log k(T)$ on $1/T$. In the same figure
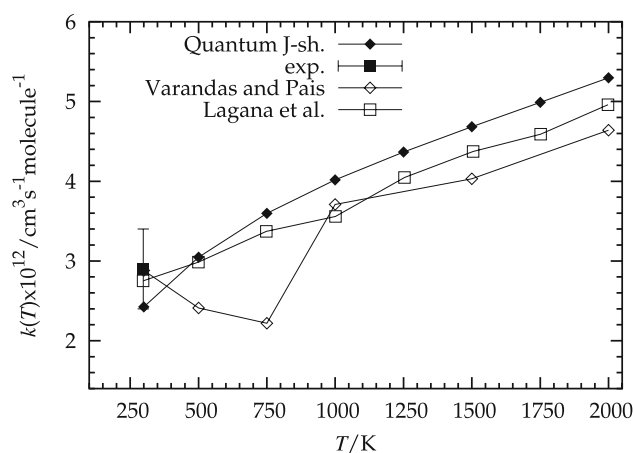

Fig. 5 Quantum J-shifting thermal rate coefficients for the O + O₂ exchange reaction compared to QCT [5, 6] and experimental values [9]

experimental values [9] and QCT results of [5] and [6] are also shown. All theoretical predictions fall within the error bars of the experiment for which a measure taken at about 300 K [9] is also shown. Quantum results confirm that the low temperature minimum found by Varandas and Pais [5] when calculating $k(T)$ is not realistic and might have been caused by an insufficient statistics of the trajectory ensemble used for the calculations. They also confirm that QCT results (whose error bar is $\pm 0.2 \times 10^{-12}$ cm³ s⁻¹ molecule⁻¹) are in substantial agreement with the J-shifting quantum ones, which are however still model dependent. In fact while the larger QCT reactivity at low temperature can be attributed to a zero point energy effect (the absence of a barrier makes all the available energy disposable for reaction), the larger quantum J-shifting reactivity at higher temperature can be attributed (as it has been found elsewhere [26, 27]) to the missing gradual distortion of the reactivity (as energy increases) in the J-shifting model.

5 Conclusions

The possibility of carrying out extended calculations on the segment of the EGEE Grid available to the COMPCHEM VO has allowed us to base the evaluation of the reactive rate coefficients of the fairly heavy O + O₂ system on the exact integration of the $J = 0$ quantum reactive scattering equations. In this way, it was possible to compare calculated thermal rate coefficients with the experiment. It was also possible to carry out tests for investigating the effect of enforcing spin symmetrization on the estimated values of the probabilities. A rationalization of the results obtained has also been attempted. In particular, excitation functions calculated at different partitioning of the internal energy

were analyzed in terms of different reaction paths singled out in plots of the interaction drawn using unconventional contour maps. The key result of the investigation was the evidence for a competition between two alternative reaction paths leading to opposite behaviours at low and high collision energy.

References

1. Levine RD, Bernstein RB (1987) Molecular reaction dynamics and chemical reactivity. Oxford University Press, New York
2. Honvault P, Launay JM (2004) In: Laganà A, Lendvay G (eds) Theory of chemical reaction dynamics. Kluwer, Dordrecht
3. Liu X, Lin JJ, Harich S, Schatz GC, Yang X (2000) Science 289:1536
4. Pais AACC, Varandas AJC (1988) J Mol Struct: THEOCHEM 166:335
5. Varandas AJC, Pais AACC (1988) Mol Phys 65:843
6. Laganà A, Riganelli A, Ochoa de Aspuru G, Garcia E, Martinez M T (1996) In: Capitelli M (ed) Molecular physics and hypersonic flows. Kluwer, Dordrecht
7. Laganà A, Riganelli A, Ochoa de Aspuru G, Garcia E, Martinez MT (1998) Chem Phys Lett 228:616
8. Esposito F, Armenise I, Capitta G, Capitelli M (2008) Chem Phys 351:91
9. Andersen SM, Klein FS, Kaufman F (1985) J Chem Phys 83:1648
10. Chapman S, Gelb A, Bunker DL (1975) Quantum Chemistry Program Exchange 273
11. Skouteris D, Castillo JF, Manolopoulos DE (2000) Comp Phys Comm 133:128
12. Enabling Grids for E-Science in Europe. http://eu-egee.org. Accessed 22 Oct 2008
13. Laganà A, Riganelli A, Gervasi O (2006) Lect Notes Comp Sci 3980:665
14. Varandas AJC (1984) Mol Phys 53:1303
15. Pastrana MR, Quintales LAM, Brandao J, Varandas AJC (1990) J Phys Chem 94:8073
16. Laganà A (1980) Comp Chem 4:137
17. Varandas AJC (1987) Chem Phys Lett 138:455
18. Garcia E, Laganà A (1985) Mol Phys 56:621
19. Laganà A, Spatola P, Ochoa de Aspuru G, Ferraro G, Gervasi O (1997) Chem Phys Lett 267:403
20. Laganà A (2004) In: Laganà A, Lendvay G (ed) Theory of chemical reaction dynamics. Kluwer, Dordrecht
21. Laganà A, Crocchianti S, Faginas Lago N, Pacifici L, Ferraro G (2003) Collect Czech Chem Commun 68:307
22. Schatz GC (1988) Chem Phys Lett 150:92
23. Pack RT, Parker GA (1987) J Chem Phys 87:3888
24. Bowman JM (1991) J Chem Phys 95:4960
25. Clary DC (1984) Mol Phys 53:3
26. Piermarini V, Crocchianti S, Laganà A (2002) J Comp Meth Sci Eng 2:361
27. Aoiz F J, Saez-Rabanos V, Martinez-Haya B, Gonzalez-Lezana T (2005) J Chem Phys 123:094101